European Journal of Medicinal Chemistry 289 (2025) 117452

Contents lists available at ScienceDirect

European Journal of Medicinal Chemistry

journal homepage: www.elsevier.com/locate/ejmech

Research paper

Rationally designed peptides inhibit the formation of α-synuclein fibrils and oligomers

Tariq T. Ali [a], Madiha Merghani [b], Mohammed Al-Azzani [b], Luisa Maria Gatzemeier [b], Michael Hoppert [c], Dora Kaloyanova [d], Tiago F. Outeiro [b,e,f,g], Piotr Neumann [h], Blagovesta Popova [a,**], Gerhard H. Braus [a,*]

[a] Department of Molecular Microbiology and Genetics, Institute of Microbiology and Genetics, University of Göttingen, Grisebachstr. 8, 37077, Göttingen, Germany
[b] University Medical Center Göttingen, Department of Experimental Neurodegeneration, Center for Biostructural Imaging of Neurodegeneration, Waldweg 33, 37073, Göttingen, Germany
[c] Department of General Microbiology, Institute of Microbiology and Genetics, University of Göttingen, Grisebachstr. 8, 37077, Göttingen, Germany
[d] Department of Biomolecular Health Sciences, Faculty of Veterinary Medicine, Utrecht University, Yalelaan 2, 3584 CM, Utrecht, the Netherlands
[e] German Center for Neurodegenerative Diseases (DZNE), Von-Siebold-Str. 3a, 37075, Göttingen, Germany
[f] Translational and Clinical Research Institute, Faculty of Medical Sciences, Newcastle University, Framlington Place, Newcastle Upon Tyne, NE2 4HH, UK
[g] Max Planck Institute for Multidisciplinary Sciences, Am Faßberg 11, 37077, Göttingen, Germany
[h] Department of Molecular Structural Biology, Institute of Microbiology & Genetics, University of Göttingen, Justus-von-Liebig-Weg 11, 37077, Göttingen, Germany

ARTICLE INFO

Keywords:
Alpha-synuclein
Parkinson disease
Alpha-synuclein oligomerization
Protein aggregation
Peptide drug discovery
Rational peptide design

ABSTRACT

Parkinson's Disease (PD) is characterized by the pathological aggregation of α-synuclein (αSyn) into oligomers and amyloid fibrils, making αSyn aggregation a key target for drug development. Peptides have gained recent attention as potential agents to inhibit aggregation. Two previously identified peptide inhibitors, discovered through large-scale yeast screening, were used as templates for *in silico* mutagenesis aimed at designing novel peptides with improved efficacy in inhibiting αSyn aggregation and cytotoxicity. The newly designed peptides underwent *in silico* docking analysis, and the most promising candidates were tested *in vitro* and in cellular models. Peptides T02 and T05 emerged as the most effective inhibitors, with T02 binding αSyn monomers and T05 targeting lower-order oligomers. Both peptides reduce αSyn fibril and oligomer formation *in vitro* and significantly suppress αSyn aggregation and cytotoxicity in yeast and human H4 cells. These novel peptides represent antagonists of αSyn aggregation with promising potential for therapeutic intervention for PD.

1. Introduction

The misfolding and subsequent aggregation of proteins is a hallmark event in a variety of neurodegenerative diseases, including Parkinson's Disease (PD) [1]. PD is the second most common neurodegenerative disorder, with approximately 1 % of the population over the age of 60 years affected, and its prevalence is steadily increasing in an aging society [2]. PD exhibits clinical motor and non-motor symptoms, resulting primarily from the degeneration of dopaminergic neurons, located in the *substantia nigra pars compacta* of the brain [3]. This neuronal loss is driven by the aggregation of α-synuclein (αSyn) into oligomers and amyloid fibrils, which subsequently accumulate into Lewy bodies (LBs) or Lewy neurites [4]. Missense mutations in the αSyn encoding *SNCA* gene [5–10], as well as gene multiplications [11,12] are known causes for αSyn aggregation. However, the majority of PD cases are of spontaneous origin [2]. αSyn is normally a soluble or membrane-associated protein, but can also misfold and form on-pathway oligomers, which can perform transitions into different amyloid fibrils. Alternatively, αSyn monomers can form toxic off-pathway oligomers [13]. Multiple reports have shown that oligomeric and protofibrilar states of αSyn are major contributors to neurodegeneration [14,15]. Misfolded αSyn species disrupt multiple cellular pathways resulting in impairment of lysosomal and proteasomal protein degradation, mitochondrial dysfunction, synaptic vesicle trafficking defects or membrane damage [16]. αSyn oligomers and fibrils can function as "seeds" for αSyn propagation to neighboring cells [17]. Thus, targeting αSyn aggregation

* Corresponding author.
** Corresponding author.
E-mail addresses: bpopova@gwdg.de (B. Popova), gbraus@gwdg.de (G.H. Braus).

https://doi.org/10.1016/j.ejmech.2025.117452
Received 8 January 2025; Received in revised form 20 February 2025; Accepted 24 February 2025
Available online 26 February 2025

represents an important therapeutic strategy to slow or halt disease progression.

The pathological pathway of αSyn assembly is a multistep process that involves a transition from the natively unfolded αSyn state to a β-sheet conformation, which stabilizes the resulting aggregates [1]. Commonly, the aggregation of proteins into amyloid fibrils has been described as a three-stage process, consisting of a lag phase, also referred to as the nucleation phase, elongation phase, and stationary phase [18]. Drug design and structure determination via X-ray crystallography or cryo-electron microscopy is challenging, due to the nature of unfolded proteins. However, structures of various αSyn amyloid fibrils have been characterized [19,20]. αSyn can form fibrils that exhibit distinct structural variations, commonly referred to as "strains" or "polymorphs." These polymorphs exhibit variations in folding patterns and intermolecular arrangements, leading to diverse fibril morphologies. αSyn polymorphs share a similar structure, where the central hydrophobic non-amyloid β component (NAC) region folds into a β-sheet, whereas C- and N-terminal regions of the protein remain unfolded [20]. Multiple research efforts are focusing on the identification of aggregation inhibitors such as small compounds that inhibit αSyn aggregation [21,22], or the rational design of peptides that interact with growing αSyn fibrils to further prevent aggregation and seeding [23,24].

Peptide-based drugs have emerged as a promising alternative to small molecules for developing disease-modifying therapies against αSyn aggregation [25]. The complex protein-protein interactions involved in the amyloid aggregation pathway typically occur over broad surface areas, making them challenging targets for small molecules. In contrast, short peptides offer high specificity for the target, thereby minimizing interfering off-target effects commonly associated with small molecule drugs [26]. Peptide drugs have the advantage that they often exhibit low toxicity and a reduced likelihood of triggering immune responses, due to their natural origin. Peptide inhibitors designed to prevent α-synuclein (αSyn) aggregation have been developed using comprehensive *in silico* modeling and interaction prediction approaches [23,24]. Recently, we screened a peptide library of approximately one million members using two high-throughput approaches in yeast. The two peptides, K84s (25 amino acids) and K102s (19 amino acids) were identified as inhibitors of αSyn oligomerization and aggregation at sub-stoichiometric molar ratios [27]. Both K84s and K102s efficiently reduced αSyn aggregation *in vitro*, and K84s additionally reduced αSyn aggregation in human neuroglioma (H4) cells.

This study provides an optimization of K84s and K102s peptide sequences through *in silico* mutagenesis with the goal to promote the formation of stable secondary structure elements. Subsequent docking calculations of the redesigned peptides were conducted using the atomic structure of αSyn fibril as a template target [28]. The major achieved aim was to provide novel peptides with enhanced efficacy in inhibiting αSyn aggregation and cytotoxicity. Four novel peptides could be identified, which efficiently inhibited αSyn oligomerization and fibrilization *in vitro*. Three peptides reduced the aggregation and αSyn-associated cytotoxicity in yeast, as well as in human H4 cells. These peptides hold significant potential as therapeutic agents against αSyn aggregation.

2. Results

2.1. Rational design of αSyn peptide inhibitors

Docking calculations were performed to elucidate how the peptides K102s and K84s [27] could interact with αSyn to inhibit its aggregation. The atomic structures of both peptides prior to docking were predicted. The AbInitio suite of ROSETTA [29] was applied, which utilizes short sequence-based fragment libraries calculated by the Robetta server [30]. Predicted models of both peptides revealed distinct secondary structure elements (Fig. 1). The cryo-EM atomic structure of αSyn fibrils was used as a template (PDB 6A6B [28]) for the ROSETTA suite docking calculations. Amino acids with side chains oriented towards the αSyn fibril, along with secondary structure elements, were identified as critical mediators of peptide-fibril interactions. The K102s peptide, in particular, contains three arginine residues and a leucine residue, which facilitate the formation of an α-helical secondary structure. Its sequence includes four amino acid residues with positively charged side chains. They align with surface regions of the αSyn fibril exhibiting a negative electrostatic potential. Additionally, the hydrophobic side chain of a tryptophan residue further stabilizes the peptide's orientation by interacting with the fibril surface. The predicted interaction region of this peptide is located between the N-terminal [50-HGVATVAEK-58] β-sheet and the [72-TGVTAV-77] region of the non-amyloid component (NAC) within a single protofibril (Fig. 1A, Fig. S1A).

The peptide K84s is composed of amino acids that favor a β-sheet conformation. It interacts with the surface of αSyn forming the cleft between the two αSyn protofibrils, which contains the two N-terminal β-sheets [50-HGVATVAEK-58] (Fig. 1B, Fig. S1B). The interaction

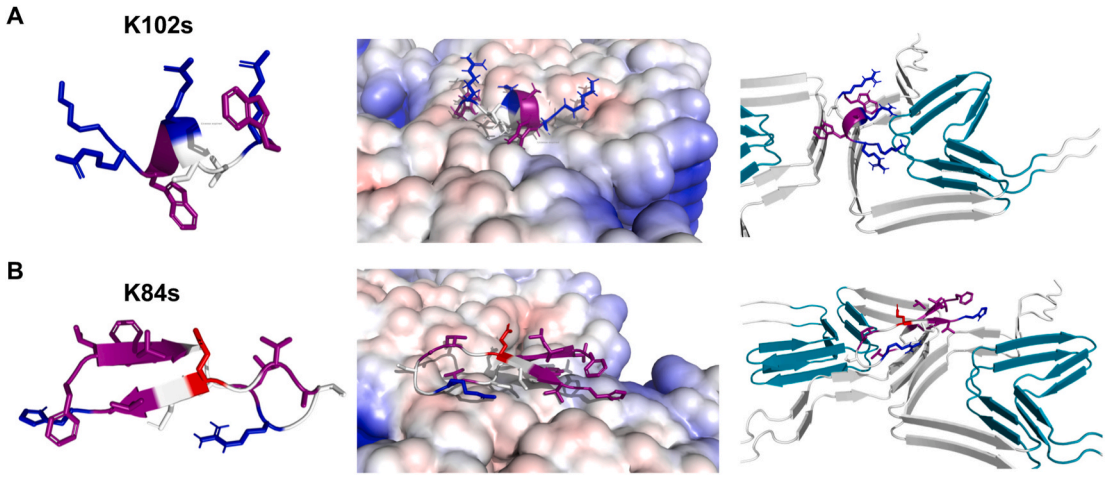

Fig. 1. Peptide secondary structure models and docking simulations. Secondary structure predictions of K102s **(A)** and K84s **(B)** were generated using the ROSETTA AbInitio suite (left panels). Positively charged, negatively charged, and hydrophobic residues are shown in blue, red, and purple, respectively. Electrostatic surface potentials (middle panels) and main chain cartoon representation (right panels) of αSyn fibril in complex with the corresponding peptides were obtained by molecular docking simulations of the interaction of K102s or K84s with αSyn fibril (PDB 6A6B). K102s docks to the N-terminal region of one protofibril, whereas K84s binds to the interface between the two protofibrils. Electrostatic surface potentials are colored red (negative) blue (positive), and white (neutral). The NAC domain of αSyn is highlighted in green. (For interpretation of the references to color in this figure legend, the reader is referred to the Web version of this article.)

between K84s and the fibril surface is facilitated through β-sheet stacking, stabilized through hydrogen bonds and π-π electron interactions. In summary, this analysis of K102s and K84s peptides revealed two distinct interaction patterns with αSyn, which are determined by their sequences and secondary structure elements.

The K102s and K84s peptides were mutagenized *in silico* to design peptides with improved binding efficiency against αSyn fibrils. Residues presumed to interact with the fibril or contribute to the existing secondary structure were excluded from mutagenesis. Only peptide derivatives predicted to form stable secondary structure elements were selected for further analysis. Docking experiments were performed with the ROSETTA suite followed by rigid-body docking. The two top-scoring derivatives of K102s and K84s, identified based on their calculated interface score (ISc), are presented in Table 1. These derivatives retain the central amino acid sequence of their precursors (underlined), whereas their altered flanking regions exhibit significant similarities to each other. Modifications to the flanking regions were designed to promote the elongation of secondary structure elements, enhancing their stability. Incorporating amino acids with similar properties on either side of the central sequence produced peptides with more energetically favorable interactions with the αSyn fibril compared to their precursors. Predicted atomic models indicate that the K102s derivatives, T02 and T03, adopt an elongated α-helical structure (Fig. 2). They include a greater number of amino acids with electrostatically charged side chains, further stabilizing their interaction with the fibril. Additionally, the N- and C-terminal regions of these derivatives include more hydrophobic amino acids, contributing to enhanced binding affinity and structural stability. The predicted docking sites have shifted from the previously identified area towards the NAC region of one protofibril. T02 interacts specifically with the surface area near the [72-TGVTAV-77] stretch, with its hydrophobic side chains oriented towards the fibril surface (Fig. 2A, Fig. S2A). In contrast, T03 forms an extended α-helix, covering a significant portion of the NAC domain surface, along the [67-GGAVVTGVTA-76] and [87-SIAAATGFV-95] stretches, with its charged side chains primarily interacting with the fibril surface (Fig. 2B, Fig. S2B). The interactions between the K102s derivatives and the αSyn fibril are facilitated by the combination of hydrophobic side chains facing the fibril surface, and the charged side chains directed either to the aqueous solvent or charged patches on the surface. This dual interaction mechanism results in a strong and stable peptide-fibril binding.

The K84s derivatives T05 and T06 exhibit increased hydrophobicity and adopt an extended anti-parallel β-sheet structure (Fig. 2C, D, Figs. S2C and S2D). These derivatives shift their docking sites from the N-terminal β-sheet [50-HGVATVAEK-58] toward the NAC domain of αSyn. T05 is the top-scoring derivate of K84s and is predicted to dock at the surface formed by the [69-AVVTG-73] and [89-AAAT-92] β-sheets (Fig. 2C). Its C-terminal aromatic amino acids insert into the αSyn fibril. This facilitates extensive β-sheet stacking interactions between the peptide and fibril. T06 forms an anti-parallel β-sheet that stretches perpendicularly across the αSyn fibril β-sheets [48-VVHGV-52], [77-VAQKTV-82] and [84-GAGSI-88] (Fig. 2D). In contrast to T05, the majority of the hydrophobic side chains in T06 are directed towards the fibril surface. Similar to T05, the β-sheet stacking of T06 is stabilized by electrostatic interactions with the αSyn fibril surface. Docking calculations indicate that the interaction of the K84s derivatives with αSyn fibril is primarily mediated by β-sheet stacking and supported by hydrophobic interactions. All derivatives display an expanded interaction area with the αSyn fibril surface, which is reflected in improved ISc values. This enhances their binding affinity and might allow the peptides to more efficiently inhibit the aggregation of αSyn by preventing additional monomers from associating with the fibril surface.

Table 1
Designed and precursor peptides with amino acid sequences and Interface Score (ISc). The conserved amino acid sequence is underlined. ISc as calculated by Rosetta Rigid-Body docking, representing non-bonded atom pair interaction energies as well as empirical and statistical potentials.

Name	Sequence	ISc
K102s	FLKRWARSTRWG	−31,87
T02	LKEFLKRWARLLRW	−46,91
T03	WKEFLKRWARWLRW	−45,43
K84s	FLVWGCLRGSAIGECVVH	−33,03
T05	LNIRVFLVWGCLRGSAYFL	−50,48
T06	IRVFLVWGCLRGSAWFVCV	−49,36

2.2. Designed peptides inhibit αSyn aggregation in vitro

The efficacy of the designed peptides to inhibit αSyn aggregation was tested in an *in vitro* aggregation assay. Formation of fibrils was observed using the Thioflavin-T (ThT) dye, which specifically binds to amyloid fibrils. This enables quantitative analysis of aggregation kinetics. Recombinantly purified αSyn was aggregated by continuous shaking at 37°C for 60 h. Peptides were chemically synthesized and αSyn fibrilization was analyzed in the presence or absence of the corresponding peptides at molar ratios of 1:2, 1:1, 1:0.5 or 1:0.1 (αSyn:peptide). A significant decrease in αSyn aggregation was observed in the presence of all four peptides (Fig. 3A–D). T02 and T03 showed the highest potency and inhibited αSyn fibrilization about 5-fold at sub-stoichiometric molar ratio to αSyn, whereas T05 and T06 were less potent at these concentrations.

At low T06 concentrations, the ThT fluorescence intensity was similar to that of αSyn alone. However, higher molar ratios of T06 almost completely inhibited αSyn fibrillization. Peptides T02, T03 and T05 performed better than their precursors at low molar ratios, whereas T06 performed similarly (Fig. 3E, Figs. S3A and S3B). In addition to a reduction in overall amyloid fibril formation, a significant increase in the lag phase was observed for T02 and T03, which is a critical step in the aggregation process (Fig. 3F). Inhibiting the lag phase of αSyn aggregation is particularly important, as it prevents the formation of toxic oligomeric species that serve as nuclei in the aggregation process. T02, T03 and T05 showed better inhibitory effects with decreasing peptide concentrations and did not exhibit a clear dose-dependent inhibition of αSyn aggregation at low molar ratios. This may be due to the hydrophobic nature of the peptides which promotes self-aggregation at elevated concentrations, limiting their bioavailability and inhibitory potential. In contrast, T06 exhibited a dose-dependent inhibitory effect at higher concentrations, suggesting different mode of action in comparison with the other peptides.

Transmission electron microscopy (TEM) of the aggregated samples confirmed that the presence of the peptides inhibits αSyn aggregation (Fig. 3G, Fig. S3C). The resulting fibrils of the aggregation assays after 60 h at 1:0.5 molar ratios were analyzed. αSyn that aggregated alone formed abundant long fibrils. The addition of T02, T03 and T05, but not of T06, resulted in a significant reduction of fibril load and fibril length (Fig. 3H). This decrease in fibril length and abundance observed in TEM correlates to the measured ThT fluorescence and indicates that the addition of the T02, T03 or T05 synthetic peptides effectively inhibits the growth of amyloid αSyn fibrils at low molar ratios. The addition of K102 lead peptide did not result in a reduction in fibril length, but in the ThT yield, suggesting a potential morphological change in amyloid fibril structure (Fig. 3H).

The impact of the peptides on αSyn aggregation could be due to an interference with the accumulation of low molecular weight oligomeric species. Amyloid fibril formation proceeds through a number of intermediate species, and soluble low weight oligomeric species are considered the major toxic species in amyloid diseases [1]. Reducing their abundance along the aggregation pathway is a key step for mitigating the toxicity associated with αSyn aggregation. Accumulation of αSyn oligomeric assemblies was monitored at the endpoint of the aggregation assays in the presence or absence of the peptides. Immunoblotting analysis revealed αSyn SDS-stable species, migrating at 15 kDa, 35 kDa, and 70 kDa, corresponding to monomeric and various oligomeric forms

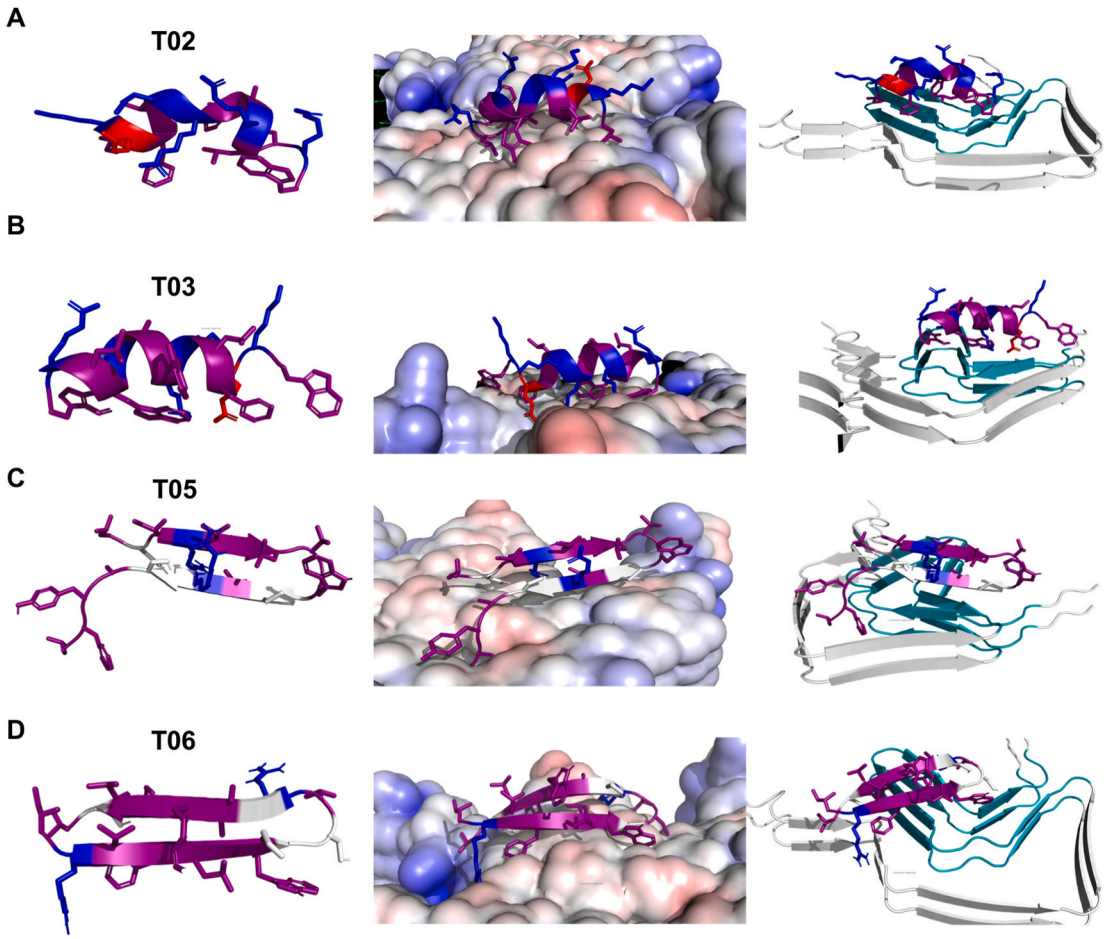

Fig. 2. Peptide secondary structure models and docking. Secondary structure predictions of K102s derivatives T02 **(A)** and T03 **(B)**, or K84s derivatives T05 **(C)** and T06 **(D)** (left panels). Electrostatic surface potentials (middle panels) and main-chain cartoon representations (right panels) show αSyn fibrils in complex with each peptide. Electrostatic potentials are colored red (negative), blue (positive), and white (neutral). The NAC domain is highlighted in green. T02 and T03 exhibit extended α-helical structures compared to K102s, while T05 and T06 derivatives of K84s maintain the anti-parallel β-sheet structure with increased β-sheet length. (For interpretation of the references to color in this figure legend, the reader is referred to the Web version of this article.)

(Fig. 4A). A notable decrease in the accumulation of these oligomeric species was observed when peptides were present (Fig. 4B). Lower molar concentrations of T05 and T06 were less effective at inhibiting the formation of these oligomeric assemblies. The high efficacy of T02 and T03 to inhibit the formation of oligomers is in line with the observation of a significantly increased lag phase. Additionally, non-denaturing dot-blot analysis of the samples using the oligomer-specific A11 antibody demonstrated that all peptides inhibit the formation of larger αSyn A11-positive oligomers (Fig. 4C). These findings corroborate that the designed peptides, which already suppress the early stages of oligomerization *in vitro*, have a strong potential to inhibit αSyn fibrilization already at low molar concentrations.

2.3. *Peptides interact with monomeric αSyn in vitro*

Far-UV circular dichroism (CD) spectroscopy was utilized to analyze the secondary structure of the synthesized peptides and to investigate their interactions with αSyn. Changes in CD spectra can reveal structural alterations resulting from such interactions. The peptides and αSyn were dissolved in 0.5 % acetonitrile at a concentration of 0.2 mg/mL, and CD measurements were conducted both individually and after mixing αSyn with the peptides (Fig. 5). T06 could not be dissolved in a solvent suitable for far-UV CD spectroscopy and was thus excluded from the analysis. The far-UV spectrum of αSyn alone confirmed its typical random coil conformation, characterized by a negative signal near 195 nm and lack of absorption signal at 210–218 nm. The secondary structure composition of the peptides with αSyn was estimated from the CD spectra using K2D3 computational method [31] and shown in Table 2. T02 (Fig. 5A) and T03 (Fig. 5B) did not exhibit any distinct secondary structure elements under the tested conditions, whereas T05 (Fig. 5C) adopted a β-sheet conformation, characterized by negative absorption peak at 218 nm. Notably, when αSyn was co-incubated with T02 or T03, significant deviations were observed between the experimental spectra and the theoretical sum of the individual spectra of αSyn and the peptides. The peak at 195 nm corresponding to random coil conformation diminished and increase of the negative peak at 218 nm was recorded. These results suggest that T02 and T03 interact with the unfolded αSyn monomers and increase the presence of β-sheet structures, which could indicate an early-stage aggregation interaction. The discrepancy between the experimental spectra and the theoretical sum of spectra suggests that αSyn and the peptides undergo conformational changes upon binding rather than behaving as independent structures. T05, which already adopts a β-sheet structure, does not induce significant further β-sheet formation upon interaction, supporting the idea that its mechanism of action might differ from that of T02 and T03.

Dynamic Light Scattering (DLS) analysis was performed to further investigate these observations. It was examined, whether the changes seen in CD spectra upon co-incubation indicate interactions between the peptides and monomeric αSyn. αSyn and the peptides were incubated either separately or together for 15 min at 37 °C, and DLS measurements were subsequently recorded (Fig. 6). The cut-off for reliable size detection was set at 1000 nm, and scattering peaks beyond this

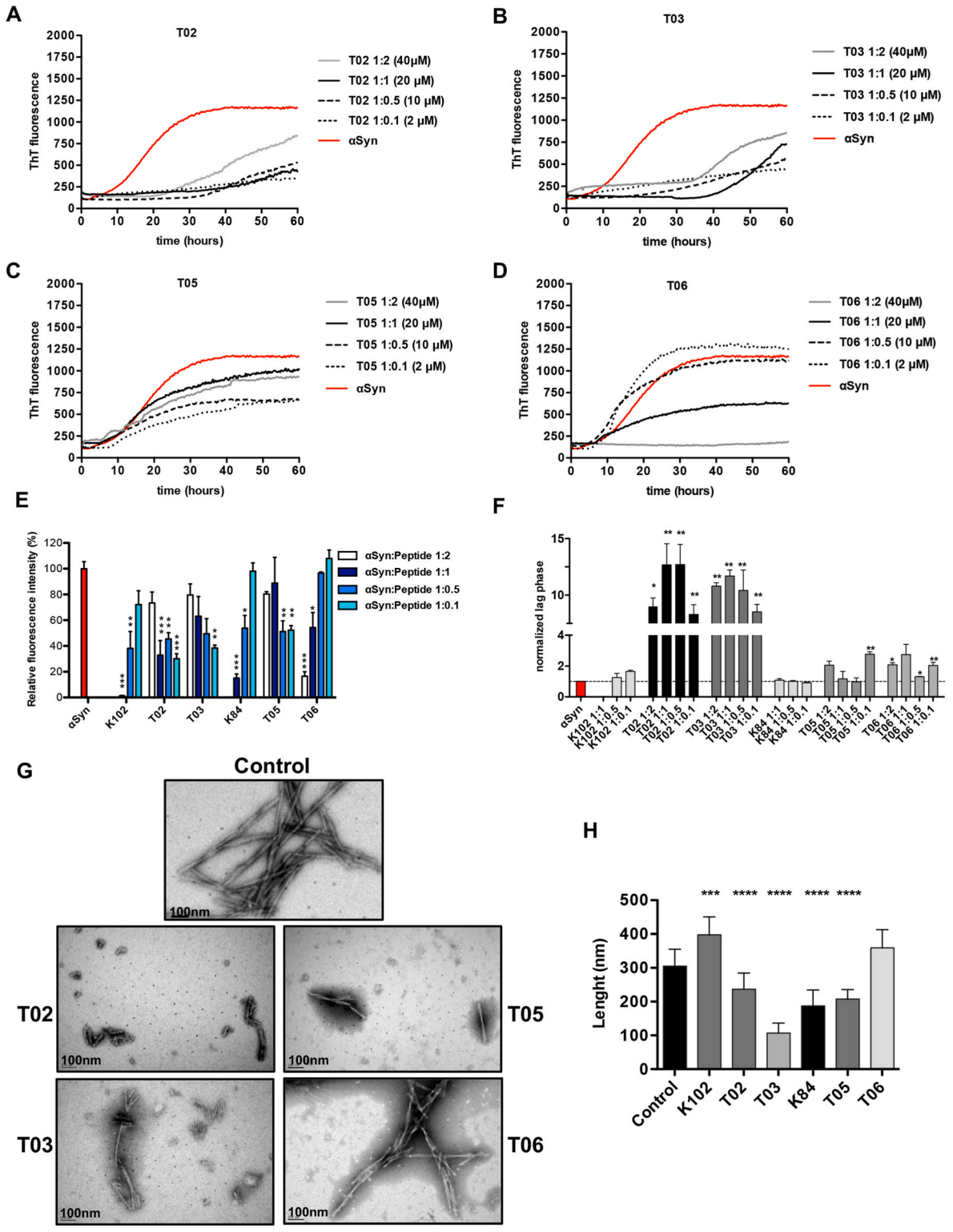

Fig. 3. Designed peptides inhibit αSyn fibrilization. (A–D) Aggregation kinetics of αSyn (20 μM) alone (red) or with T02, T03, T05, or T06 (black) over 60 h, monitored by ThT fluorescence emission. Data represent representative curves from three independent experiments. **(E)** Relative fluorescence intensity after 60 h incubation of αSyn (20 μM) with the peptides at the indicated molar ratios. **(F)** Lag phase of the aggregation reactions, normalized to αSyn alone. Significance is assessed by *t*-test (***$p < 0.001$; **$p < 0.01$; *$p < 0.05$; n = 3) **(G)** TEM images of αSyn fibrils after 60 h with or without peptides (control). **(H)** Mean fibril length quantification; significance was assessed by *t*-test (****$p < 0.0001$; ***$p < 0.001$; n = 50). (For interpretation of the references to color in this figure legend, the reader is referred to the Web version of this article.)

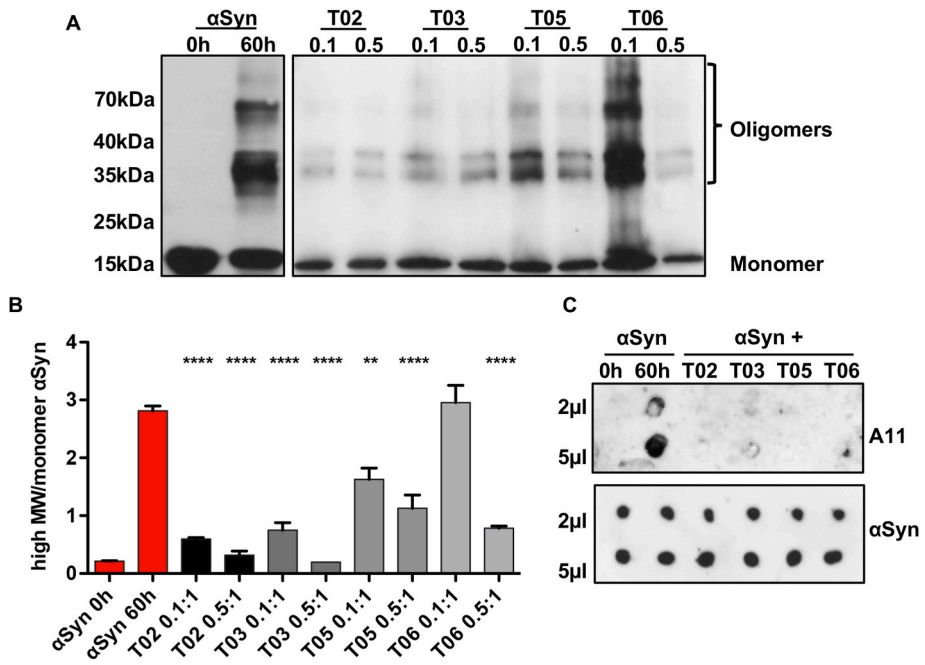

Fig. 4. Designed peptides reduce αSyn oligomerization. (A) αSyn (20 μM) was incubated alone or with the peptides at the indicated molar ratios. Samples from 0 h (control) and 60 h were analyzed by immunoblotting with anti-αSyn antibody. **(B)** Densitometric analysis of αSyn oligomer-to-monomer ratio; significance to αSyn (60 h) was assessed by *t*-test (****$p < 0.0001$; **$p < 0.01$; n = 3). **(C)** Dot-blot analysis of 60 h samples (1:0.5 αSyn:peptide) using A11 anti-oligomer antibody. The membrane was stripped and re-probed with anti-αSyn as a loading control.

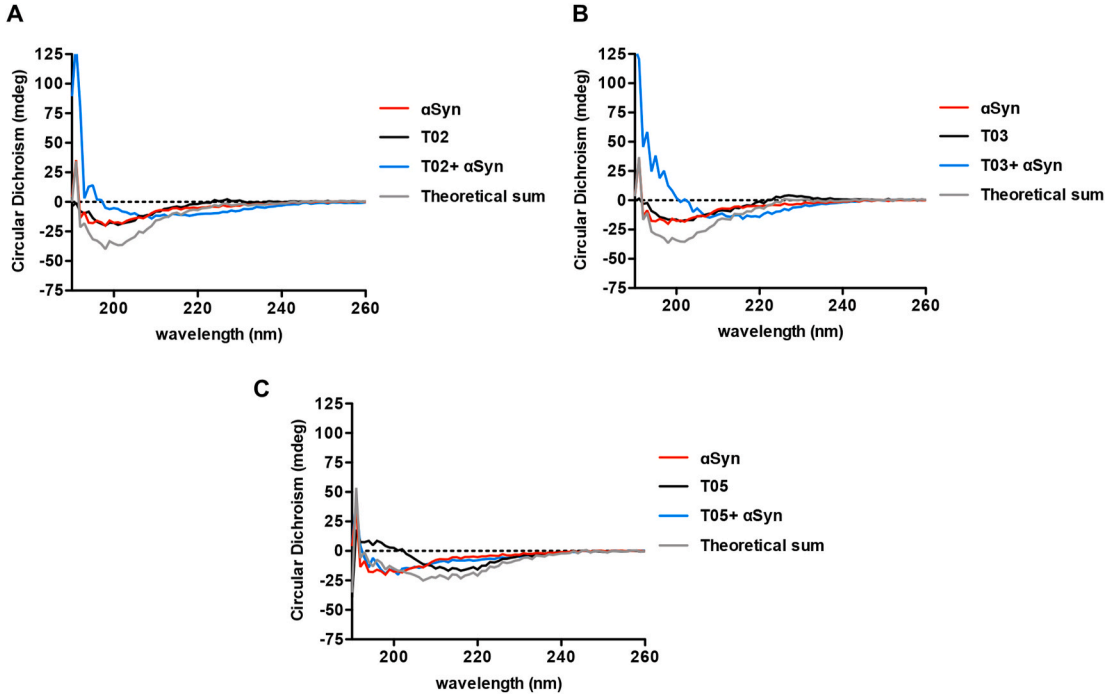

Fig. 5. Circular dichroism (CD) spectra of designed peptides with and without αSyn. Far-UV CD spectra of T02 **(A)**, T03 **(B)**, and T05 **(C)** alone (black), after incubation with αSyn (blue), and αSyn alone (red). Grey lines represent the theoretical sum of individual spectra of αSyn and the corresponding peptide. T05 alone exhibits a β-sheet secondary structure element. Co-incubation of T02 and T03 with αSyn results in spectra that deviate from the theoretical sum, indicating a structural interaction between αSyn and the peptides. Each spectrum represents the average of six recordings. (For interpretation of the references to color in this figure legend, the reader is referred to the Web version of this article.)

threshold were excluded from the analysis. In the absence of peptides, the DLS profile showed a major peak corresponding to αSyn species with a hydrodynamic radius (R_h) of approximately 3.1 nm. This is indicative for monomeric αSyn and suggests together with the observed minor peaks that also some oligomeric species are formed during incubation. Both T02 and T03 peptides exhibited peaks corresponding to small species, when analyzed individually, which likely reflect their monomeric forms in solution. When αSyn was co-incubated with the T02

Table 2
Quantification of secondary structure elements. α-helix and **β-sheet** content for peptides **T02, T03, and T05** and after co-incubation with αSyn, as determined by K2D3 analysis of CD spectra. The theoretical combined spectra represent the expected secondary structure distribution assuming no interaction between the peptides and αSyn.

	Peptides		Peptides with αSyn (co-incubation)		Theoretical combined spectra	
	% α-helix	% β-sheet	% α-helix	% β-sheet	% α-helix	% β-sheet
T02	4.38 %	17.46 %	2.94 %	26.59 %	10.74 %	18.45 %
T03	4.21 %	18.00 %	3.02 %	29.41 %	11.36 %	17.25 %
T05	2.40 %	20.36 %	4.93 %	18.17 %	19.68 %	17.07 %

peptide, a notable alteration in the DLS profile was observed, revealing a significant shift in the species distribution (Fig. 6A). The peak corresponding to monomeric αSyn diminished in intensity, and a new peak with larger hydrodynamic radius emerged, indicating an interaction between T02 and monomeric αSyn. A similar, though less pronounced interaction was observed between the T03 peptide and αSyn (Fig. 6B). In contrast, the DLS profiles of the β-sheet peptides T05 and T06 demonstrated more complex behavior. Both peptides exhibited peaks corresponding to larger R_h, consistent with the presence of oligomeric or aggregated peptide forms. T05 displayed multiple peaks representing species of varying sizes (Fig. 6C), whereas T06 formed a single prominent peak without substantial variations in hydrodynamic radius (Fig. 6D). T06 appeared to reduce the presence of monomeric αSyn. T05 did not demonstrate significant interactions with αSyn monomers and the observed alteration in the DLS profile may be attributed to interactions with αSyn oligomeric species.

In summary, T02 and T03 influence the distribution of αSyn species and interact with monomeric αSyn, suggesting a distinct mode of action when compared to the β-sheet-forming peptides T05 and T06. DLS analysis also revealed that T02 and T03 exist primarily as monomers in solution, while T05 and T06 predominantly form oligomeric species, with T06 exhibiting a single stable oligomeric form.

2.4. Expression of the peptides rescues αSyn-associated cytotoxicity and aggregation in yeast

A potential protective effect of the newly designed peptides in living cells was further evaluated. The budding yeast *Saccharomyces cerevisiae* was employed as an established eukaryotic model organism for analysis of the molecular mechanisms underlying PD as well as for drug screening. Expressing human αSyn in yeast mimics key features of PD pathology, such as toxic aggregate formation and cellular stress responses, making it a valuable tool for studying molecular mechanisms and potential therapeutic interventions [32–35]. The amino acid sequences of the peptides were converted into DNA sequences using EMBOSS Backtranseq online tool [36] and subsequently cloned into yeast vectors. αSyn was co-expressed with the peptides, and growth assays were conducted in both liquid (Fig. 7A) and solid media (Fig. 7B). Expression of αSyn alone leads to significant growth retardation, whereas co-expression with the four peptides led to suppression of αSyn-induced cytotoxicity and growth rescue.

Yeast strains with three genomically integrated copies of αSyn-GFP gene ("high-tox" strain) were examined, which result in a strong growth retardation phenotype [34]. We analyzed whether the expression of the peptides affects the aggregate formation of αSyn-GFP. Fluorescence microscopy was performed in the presence and absence of peptide expression (Fig. 7C). The numbers of cells displaying aggregates were significantly reduced upon expression of T02, T03 and T05, whereas T06 had no effect (Fig. 7D). Immunoblotting analysis with αSyn antibody revealed that αSyn protein levels in the presence or absence of peptide expression are similar, indicating that the differences are not due to

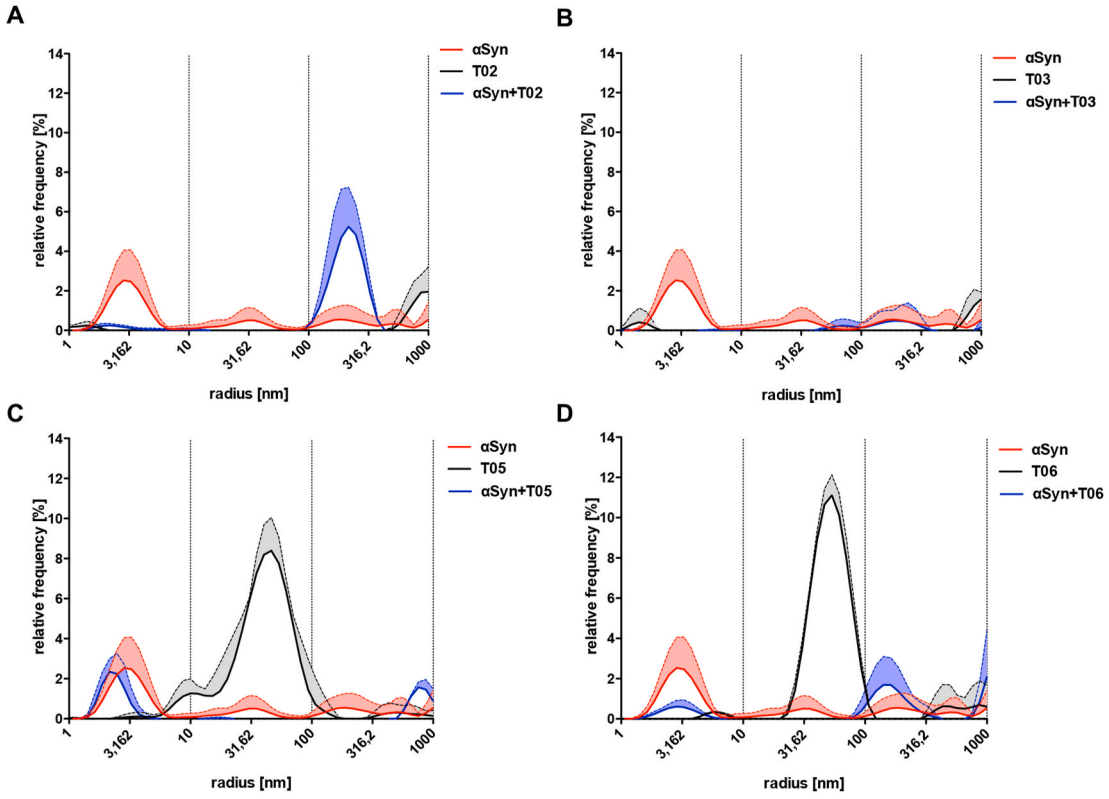

Fig. 6. Dynamic Light Scattering (DLS) analysis. DLS size distribution of T02 **(A)**, T03 **(B)**, T05 **(C)** and T06 **(D)** with or without αSyn, measured using Prometheus Panta. Plots show particle size distribution based on mean hydrodynamic radius, calculated through cumulate analysis. Shifts in particle size distributions indicate interactions or size alterations of αSyn in the presence of the peptides.

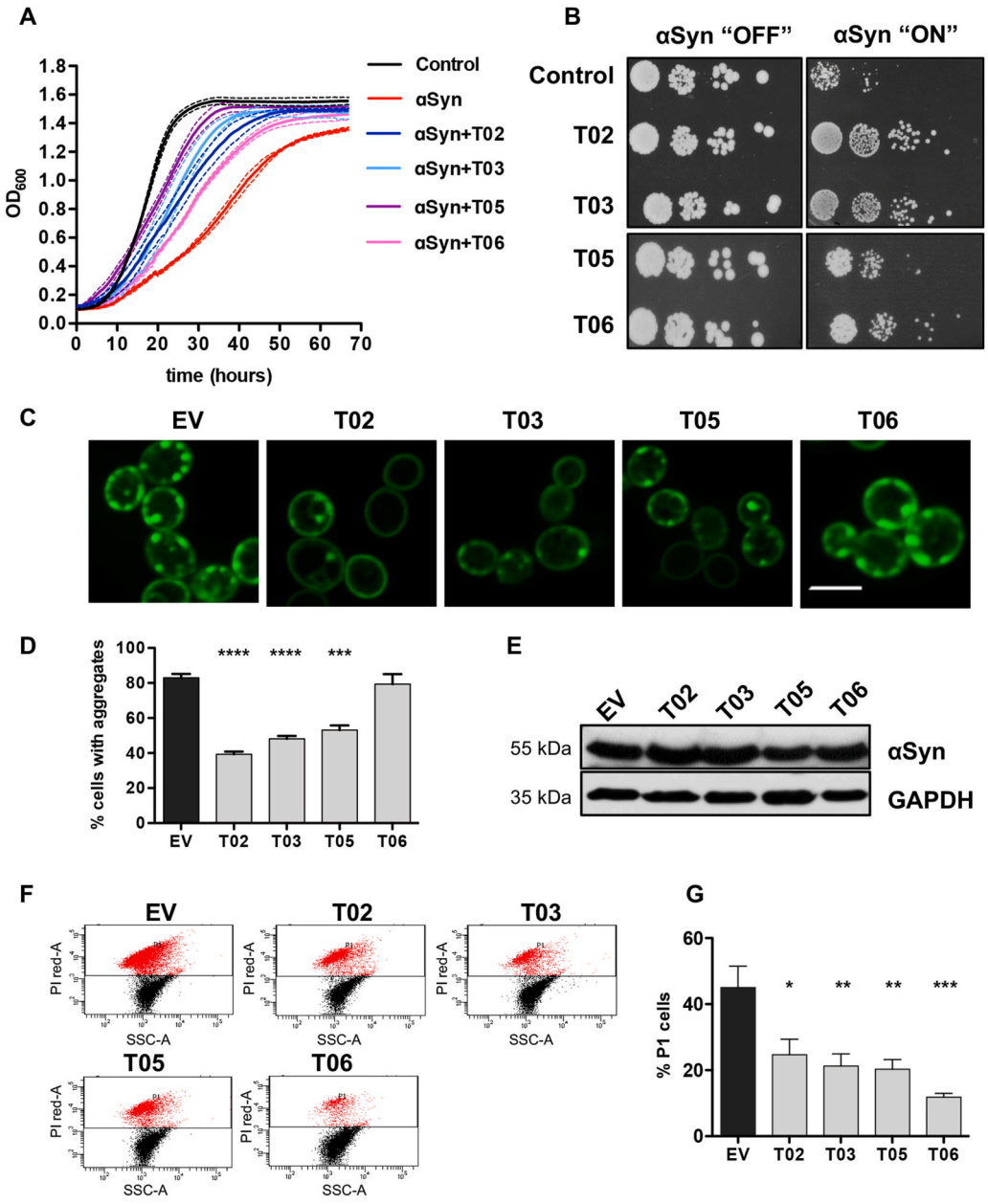

Fig. 7. Peptide expression reduces αSyn-associated growth inhibition and aggregation in yeast. (A) Growth of yeast cells expressing *GAL1*-driven αSyn from 2μ plasmid with or without the peptides. Empty vector served as control. The peptide-encoding sequences were cloned in yeast vectors and co-expressed with αSyn. **(B)** Spotting assay of yeast cells from **(A)** on selective plates with glucose (αSyn "OFF") or galactose (αSyn "ON"), imaged on day 3. **(C)** Live-cell fluorescence microscopy of high-toxicity αSyn-GFP yeast strain with or without constitutive peptide expression. Empty vector (EV) was used as control. Scale bar: 5 μm. **(D)** Quantification αSyn-GFP aggregates, co-expressing the indicated peptides. Significance of differences was calculated with *t*-test (****$p < 0.0001$; ***$p < 0.001$; n = 100). **(E)** Immunoblot of yeast extracts after 6 h galactose induction using anti-αSyn and anti-GAPDH (loading control). **(F)** Propidium iodide (PI) fluorescence measured by flow cytometry (10 000 cells) after 6 h αSyn induction. **(G)** Quantification of PI-positive cells (P1) with higher fluorescent intensities than the background from (F). Significance of differences was calculated with *t*-test relative to αSyn (*$p < 0.05$; **$p < 0.01$; ***$p < 0.001$; n = 3).

changed αSyn protein levels (Fig. 7E).

Differences in cytotoxicity, which are associated with changes in growth and aggregate formation, were determined. Propidium iodide (PI) staining was performed to assess membrane permeability, which provides a sensitive measure of yeast cell viability. Flow cytometry analysis of cells expressing both αSyn and the peptide constructs revealed a significantly lower proportion of PI-positive cells compared to cells expressing αSyn alone without peptides (Fig. 7F and G). These findings align with the growth assay data, demonstrating that the expression of the peptides substantially reduces αSyn aggregate formation and improves cell growth and viability.

The specificity of the protective effect of the peptides to αSyn was addressed. Therefore, the peptides were expressed in a yeast strain harboring the exon 1 of human huntingtin protein with 103 glutamine repeats (HttQ103). HttQ103 expression results in the formation of aggregates and is cytotoxic to yeast cells [37]. Growth analysis revealed no rescue effect in cells expressing HttQ103 in the presence of the peptides (Fig. S4A). Additionally, fluorescence microscopy of CFP-tagged HttQ103 revealed that peptide expression did not prevent HttQ103 inclusion formation (Figs. S4B and C). These findings corroborate that the peptides selectively inhibit aggregation and cytotoxicity in the context of αSyn fibril formation.

2.5. Designed peptides reduce the formation of αSyn inclusions in human H4 cells

Next, we assessed whether the designed peptides inhibit αSyn aggregation in human neuroglioma (H4) cells. The synuclein model of aggregation in H4 cells involves co-expression of C-terminally modified version of αSyn (SynT) with synphilin-1, which facilitates the formation of intracellular αSyn inclusions [38,39]. H4 cells were transfected with SynT + synphilin-1 constructs and 6 h afterward treated with 10 μM peptides. αSyn inclusion formation was assessed after 42 h by fluorescence microscopy. Expression of SynT resulted in the formation of cytosolic inclusions (Fig. 8A). Treatment of H4 cells with the peptides T02, T05 or T06 significantly reduced the number of cells with inclusions (Fig. 8B), as well as the number of inclusions per cell (Fig. 8C). T03 did not affect αSyn inclusion formation. These results revealed a strong and promising potential of peptides T02, T05, and T06 to inhibit αSyn aggregation in human cells.

3. Discussion

This study employs a novel approach for the identification of peptide-based inhibitors of αSyn aggregation. Results from high-throughput *in vivo* screening were combined with *in silico* redesign employing computational mutagenesis and docking experiments. The integration of these strategies enabled the design of specific lead peptides. These are solid and promising key prerequisites, which can be further developed for therapeutic peptide inhibitors targeting αSyn oligomerization and fibrilization in Morbus Parkinson.

Aggregation of αSyn into amyloid fibrils is a central pathogenic process in neurodegenerative diseases such as Parkinson's disease (PD) and other synucleinopathies. Oligomeric intermediates and protofibrillar structures that are formed in this aggregation process are implicated as the major source of toxicity in Parkinson's disease, and thus a potential drug target [14,15,40]. This insight underscores the need for therapeutic strategies aimed at preventing the formation of toxic oligomers and pre-fibrillar assemblies, which could potentially halt or slow the progression of neurodegenerative disorders. Recent advances in this area have focused on small natural compounds [22] and aggregation-inhibiting peptides [24,41], which each offer distinct advantages and limitations. Peptides exhibit high specificity for their targets, which reduces the risk of off-target effects and enhances safety profiles. Additionally, peptides, as naturally occurring biomolecules, are less likely to trigger adverse immune responses. Peptides also face significant challenges. This includes poor oral bioavailability, short half-life, and delivery difficulties, which have to be addressed to fully realize their therapeutic potential [42]. Despite these limitations, several peptide-based drugs have received FDA approval and are currently in clinical use, including treatments for neurodegenerative diseases [43,44], affirming their therapeutic potential.

The non-amyloid component (NAC) domain of αSyn contributes primarily to the amyloid fibril formation. Especially, the hydrophobic amino acids and β-sheet stacking motifs promote the stabilization of amyloid structures. Rational design efforts to inhibit αSyn aggregation have largely utilized the NAC domain as a structural template to develop peptide inhibitors [24]. In this study, two peptides were used as templates that we had previously identified in a large-scale *in vivo* screen for inhibitors of αSyn aggregation [27], which do not share sequence homology with the NAC domain. Both peptides were subjected to *in silico* redesign approaches. Non-interaction-contributing amino acids were targeted to enhance binding specificity and stability. Modifications were performed using *in silico* tools to predict optimal amino acid substitutions. Subsequent docking studies on the atomic structure of the αSyn fibril identified top-scoring peptide derivatives. They were synthesized and further validated *in vitro* and in cellular models to evaluate their efficacy against αSyn aggregation. Protein-protein interactions often depend on a limited number of key residues. This allows the generation of a large pool of *in silico* mutant versions, which can be efficiently screened by docking against the αSyn fibril. Stacking of hydrophobic face sites is a common mechanism in amyloid formation and can be exploited in the design of aggregation inhibitors. The top-scoring peptide derivatives exhibited elongated secondary structural elements and a higher proportion of hydrophobic residues, which emerged as a

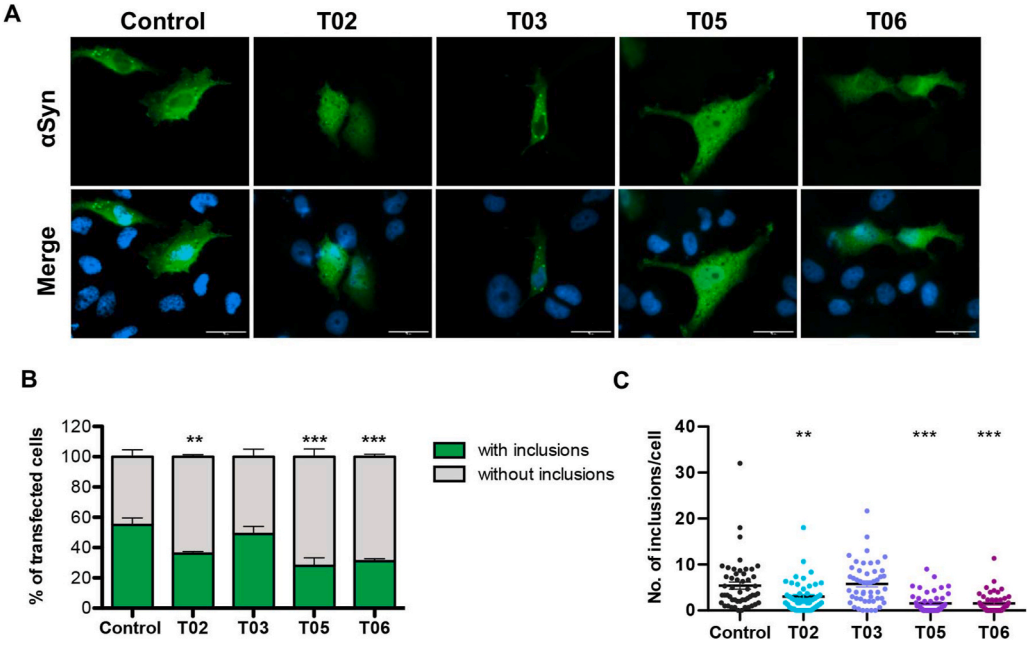

Fig. 8. Peptides reduce the formation of αSyn inclusions in human cells. (A) Fluorescence microscopy images of human neuroglioma (H4) cells expressing αSyn. H4 cells were transfected with SynT and synphilin-1 encoding constructs, and treated with the corresponding peptides (10 μM) or DMSO (vehicle control) for 48 h. Cells were fixed and αSyn was stained using immunocytochemistry. Nuclei were stained with DAPI. Scale bar = 30 μm **(B)** Percentage of transfected cells with αSyn inclusions upon treatment with the peptides or vehicle control **(C)** Number of αSyn inclusions per cell. Statistical significance was calculated using *t*-test relative to the control (**$p < 0.01$; ***$p < 0.001$; n = 3).

common feature driving interaction with αSyn. The high abundance of hydrophobic amino acids helps direct the peptides towards the similarly hydrophobic surface of αSyn.

Peptides T02 and T03 include charged side-chain residues positioned either towards areas of the αSyn fibril with opposite surface potential or towards the aqueous solvent. Conversely, T05 and T06 form anti-parallel β-sheets, which facilitate interactions with αSyn fibril through β-sheet stacking. The increased number of amino acid residues involved in the productive inter-molecular (pepide-αSyn) interactions, along with enhanced hydrophobicity correlates with higher binding affinities predicted *in silico*. While the docking calculations did not reveal specific residue-to-residue interactions, they suggest that the interactions are primarily driven by β-sheet stacking, electrostatic forces, and hydrophobicity effects. Further peptide optimization can follow in a similar workflow, using *in silico* approaches to generate and screen a larger peptide library against αSyn. Increasing amino acids with properties favoring these interactions may enhance docking efficacy. However, larger peptides could pose challenges in drug development, particularly in cellular uptake and delivery. Notably, we propose that the lack of specific residue-to-residue interactions between peptides and αSyn is crucial in preventing aggregation at the pre-oligomeric or early oligomeric stage. This hypothesis is supported by the observation that β-sheet-forming peptides interact with both early-stage oligomers and mature fibrils - structures predominantly composed of αSyn in β-sheet conformation - facilitating the β-sheet stacking seen in docking simulations. In contrast, T02 and T03, which interact with both monomeric αSyn and amyloid fibrils, do not require a specific structural conformation for binding, relying instead on hydrophobicity and electrostatic interactions. This mode of binding allows interaction even in the absence of fully formed β-sheets or oligomers. A recent study designed bis-chalcone polyphenol compounds to inhibit αSyn aggregation and disaggregate preformed fibrils [45]. These polyphenols act through strong hydrogen bonding, π-stacking, and hydrophobic interactions with αSyn residues, effectively extending the lag phase and interfering with β-sheet formation. While our rationally designed peptides also target αSyn aggregation, they differ in mechanism. Polyphenols stabilize αSyn in its monomeric or oligomeric form by directly engaging aggregation-prone domains, whereas our peptides selectively bind αSyn monomers (T02) or oligomeric species (T05) to prevent further fibrillation.

Aggregation assays using Thioflavin T (ThT) measurement with recombinant αSyn demonstrated that the designed peptides reduced amyloid fibril formation by up to 80 % at sub-stoichiometric concentrations. The peptides exhibited different dose-dependent behaviors, with T02, T03, and T05 showing stronger inhibition with decreasing concentrations. This effect may be attributed to the non-linear behavior of peptide interactions with αSyn. Peptides can exhibit non-monotonic effects at different concentrations, which is often seen with compounds that aggregate at higher concentrations, reducing their effective activity [46]. At low concentrations, the peptides efficiently interact with αSyn, but self-aggregation at higher levels may limit their availability. In contrast, T06 displayed a dose-dependent inhibition with increasing concentrations. We propose that T06 oligomers, which are more abundant at higher molar ratios, interact with αSyn in its monomeric and early oligomeric states. Transmission electron microscopy corroborated the results from the ThT assays since it showed a marked reduction in fibril length and abundance. Further analysis revealed that the peptides not only diminished amyloid fibril formation but also reduced the presence of various oligomeric αSyn species. Notably, A11-positive oligomers were undetectable when αSyn was incubated with the designed peptides. Previous studies have identified A11-positive oligomers, which are larger than soluble oligomers, as key contributors to cytotoxicity in PD [47]. These findings strongly support that the peptides effectively inhibit aggregation at the transition from monomeric αSyn to lower oligomeric species.

The ability of rationally designed peptides to inhibit αSyn aggregation without leading to accumulation of oligomers or small fibrils is critical in considering them as potential therapeutic agents, as these intermediates of αSyn aggregation are recognized as highly toxic [14,15,48]. Dynamic light scattering (DLS) analysis revealed interactions between the peptides and monomeric αSyn. Peptides T02 and T03 showed strong evidence of monomer interaction, whereas T05 and T06, which form β-sheets, exhibited either no detectable interaction (T05) or partial interaction (T06) with monomers. The aggregation assays and DLS findings suggest that interactions with lower oligomeric species are likely for T05 and T06. The different interaction patterns observed between α-helical and β-sheet-forming peptides highlight the structural specificity of their effects on αSyn aggregation.

The inhibitory effects of these peptides on αSyn aggregation extended to *in vivo* models. Further analysis of the peptides was performed in *S. cerevisiae*, a well-established PD reference organism [33,34]. Peptide co-expression in yeast reduced cytoplasmic αSyn aggregates, correlating with improved cell growth and viability, key indicators of αSyn cytotoxicity in the yeast model. In human H4 neuroglioma cells, peptides significantly decreased the number of cells with αSyn inclusions and reduced inclusion counts per cell. The ability of the designed peptides to reduce the formation of αSyn inclusions in human cells is an important verification of the aggregation inhibiting properties of the peptides. Remarkably, β-sheet peptides demonstrated stronger effects, whereas T03 failed to reduce inclusions. These findings raise important questions regarding cellular peptide uptake and intracellular stability. Our study provides strong evidence for the efficacy of rationally designed peptides in inhibiting αSyn aggregation and cytotoxicity, suggesting that they maintain functional stability at relevant biological timescales. However, further investigations are needed to evaluate their pharmacokinetic and pharmacodynamic properties. A key challenge in peptide-based therapeutics is their stability in biological environments, particularly in cellular and *in vivo* settings. Additionally, the ability of these peptides to cross the blood-brain barrier (BBB) remains an open question. Future studies will explore the use of cell-penetrating peptides or other modes of transport to enhance BBB permeability, followed by validation in physiologically relevant BBB models.

The peptides developed in this study exhibit strong aggregation-inhibiting effects, particularly by reducing αSyn oligomers and amyloid fibrils. *In silico* redesign, combined with *in vitro* and *in vivo* analysis, highlights the importance of hydrophobicity and the existence of secondary structure elements in mediating peptide-αSyn interactions. Small modifications in peptide flanking regions can significantly alter their inhibitory properties. This supports a promising potential for further optimization towards peptide drugs. Addressing these challenges will be essential for advancing these peptides as potential drugs. The ability of these peptides to prevent oligomer formation is particularly noteworthy from a therapeutic perspective, as αSyn oligomers and pre-fibrillar species are implicated in cellular seeding and disease propagation [17,49]. Our findings lay a solid foundation for the optimization of peptide-based drugs targeting early stages of αSyn aggregation in neurodegenerative diseases.

4. Experimental

4.1. Computational design of peptide inhibitors

Peptides K84s and K102s [27] were subjected to semi-rational *in silico* mutagenesis, substituting all amino acids not predicted to interact with αSyn with amino acids that are promoting formation of either α-helices or β-strands. A variety of peptide lengths of the lead peptides were generated initially, with the best scoring option being used for further *in silico* mutagenesis. This resulted in 65535 derivatives of K102s and 3375 derivatives of K84s. The secondary structure of the derivatives was determined using a local installation of PSIPRED V4.1 utilizing filtered non-redundant protein sequence data bank (UNIREF90, http

://www.uniprot.org/). Peptides with the most stable predicted secondary structure were used for global prediction using CLUSPRO [50] and subsequently refined using high resolution rigid body docking and refinement using ROSETTA [51,52]. Generated docking decoys were ranked based on the ROSETTA Interface score (ISc). Initial docking prediction was performed against αSyn fibril deposited as PDB: 6A6B [28].

4.2. Peptide synthesis

Peptides T02, T03, T05 and T06 were synthesized using Microwave-assisted solid-phase peptide synthesis (MW-SPPS) [53] using a Liberty Blue™ peptide synthesizer (CEM, Kamp-Lintfort, Germany) in 0.05 mmol scale. Peptides were purified using preparative high-performance liquid chromatography and characterized by ultra-high-performance liquid chromatography (Fig. S5) and electrospray ionization (high--resolution) mass spectrometry (ESI-(HR)MS) (Supplementary Figs. S6–S9). The protocol used for the automated MW-SPPS and peptide analysis is described in Supplementary Information.

4.3. Thioflavin T assay

Thioflavin T (ThT) assay was modified from Ref. [54] using 20 μM αSyn in a buffer containing PBS, 1 mM EDTA, 150 mM NaCl, 0.002 % SDS and 30 μM ThT (Sigma-Aldritch, St. Louis, MO). αSyn was incubated in the absence or presence of peptides at the indicated molar ratios for 60 h at 37 °C with continuous shaking in a black 96-well microplate (Invitrogen, Eugene, OR) pre-loaded with one glass bead per well. Each well was loaded with a total volume 100 μL, and the fibril formation was monitored by fluorescence using excitation at 440 nm and emission at 480 nm with a Tecan Infinite M200 plate reader (Tecan, Switzerland). αSyn that was incubated without peptides was used as a negative control and all measurements were carried out in triplicates.

4.4. Circular dichroism spectroscopy

Circular dichroism (CD) spectra of the peptides and αSyn at a concentration of 0.2 mg/mL were recorded in the far UV region (190–260 nm). The peptides were diluted in 0.5 % acetonitrile. Secondary structure of αSyn and peptides in the presence or absence of αSyn was analyzed by measuring the circular dichroism in mdeg in the far UV spectra. Six average scans were performed using a 0.1 cm cuvette and were collected with a Chirascan (Applied Photophysics Ltd., Leatherhead, U.K.) using the associated Chirascan software. Secondary structure distribution was evaluated using the K2D3 online server [31], using the ellipticity measured as input.

4.5. Dynamic light scattering

Isothermal Dynamic Light Scattering (DLS) measurements were conducted using a Prometheus Panta instrument (NanoTemper Technologies GmbH, Munich, Germany) to assess particle size distributions. The peptides T02, T03, T05 and T06 were diluted in PBS to a final concentration of 180 μM individually, or in combination with 90 μM αSyn. The samples were incubated for 15 min at 37°C and loaded into High Sensitivity glass capillaries (10 μL each). Measurements were carried out at 37°C in triplicates of ten consecutive DLS measurements of each capillary taken at 20 % LED power, 100 % Laser power. The hydrodynamic radius (R_h) of the particles was calculated using the software associated with the Prometheus Panta system.

4.6. Transmission electron microscopy

αSyn aggregation products were analyzed by transmission electron microscopy (TEM) of negatively strained samples prepared according to Ref. [55]. In brief, the aggregation products resulting from the incubation with or without peptide inhibitors in a ratio of αSyn to peptides of 1:0.5 were transferred onto a thin carbon film, previously evaporated onto a freshly cleaved mica surface, and washed with ultrapure water to remove the aggregation buffer. The sample on the carbon film was stained using 3 % (w/v) phosphotungstic acid (pH 7.0) and the film was picked up using an electron microscope grid (300 mesh, Plano, Wetzlar Germany). Excess staining liquid was immediately removed. The prepared sample was imaged using a Jeol EM 1011 transmission electron microscope (Jeol, Eching, Germany) and a Gatan Orius 4 K camera (Gatan, Munich, Germany). Multiple images per sample were taken and 50 individual fibrils were measured to access fibril length.

4.7. Immunoblotting

Cells expressing αSyn and the peptides were grown over night at 30 °C in selective SC medium containing 2 % raffinose and inoculated the next day at an $OD_{600} = 0.3$ in selective SC medium containing 2 % galactose, to induce the expression of *GAL1*-driven αSyn. αSyn expression was induced for 6 h, while the peptides were constitutively expressed. For each sample an OD of 5 was harvested and the total protein extract was prepared using 0.25 M sodium hydroxide with 1.5 % 2-mercaptoethanol for cell lysis, and 7.2 % trichloroacetic acid for protein precipitation. Protein pellet was resuspended in 50 μL HU-loading buffer (200 mM Tris-HCl pH 6.8; 8 M Urea; 5 % SDS; 1 mM EDTA; 0.05 % bromophenol blue), and 25 μL loaded into each well. After gel electrophoresis in a 12 % SDS polyacrylamide gel, proteins were blotted into a nitrocellulose membrane (GE Healthcare, Chicago, IL). Membranes were probed with anti-αSyn mouse antibody (Becton Dickinson, Franklin Lakes, NJ), and anti-GAPDH mouse antibody (Thermo Fischer, Waltham, MA) was used as loading control. For native dot blot analysis probes from *in vitro* αSyn aggregation assays were dropped onto nitrocellulose membranes and incubated with A11 mouse antibody (Thermo Fischer, Waltham, MA) or anti-αSyn mouse antibody. Pixel density was measured from TIFF files originating from digitized X-ray films (Cytiva, Marlborough, MA) and analyzed using the ImageJ software (NIH, Bethesda, MD).

4.8. Yeast strains, transformations and growth conditions

The used strains and plasmids are listed in Tables 3 and 4. Plasmids were constructed using GENEART seamless cloning and assembly kit (Life Technologies-Ginco, Carlsbad, CA) and verified by sequencing. Yeast strains were grown on YEPD (Yeast-Extract-Peptone-Dextrose) media or on synthetic complete dropout (SC) medium, lacking the respective amino acids for selection. The medium was supplemented with either 2 % glucose, 2 % raffinose, or 2 % galactose. Yeast cells were transformed with plasmids using standard lithium acetate procedure [56].

4.9. Spotting assay

For growth test on solid medium cells were grown overnight in minimal liquid media containing 2 % raffinose, lacking the appropriate amino acid for selection. Overnight culture was diluted to $OD_{600} = 0.1$,

Table 3
Yeast strains used in this study.

Name	Description	Source
W303-1A	MAT*a, ura3–1, trp1–1, leu2–3_112, his3–11, ade2–1, can1–100*	EUROSCARF
BY4741	MAT*a, ura3Δ0, his3Δ1, leu2Δ0, met15Δ0*	EUROSCARF
RH3468	W303 containing three genomic copies of *GAL1-SNCA-GFP* in *ura3* locus	[34]
RH3788	BY4741 containing *GAL1 FLAG-htt-103Q ΔProCFPp303* in *his3* locus	[27]

Table 4
Plasmids used in this study.

Name	Description	Source
p426-GAL1	*GAL1*-promoter, *CYC1*-terminator, *URA3*, 2 μm, *AmpR*	[57]
p425-GPD	*GPD*-promoter, *CYC1*- terminator, *LEU2*, 2 μm, *AmpR*	[57]
pME3760	p426 with *GAL1::SNCA*	[34]
pME4913	pET22b-*SNCA*	[27]
pME5560	p425-GPD-T02	This study
pME5561	p425-GPD-T03	This study
pME5562	p425-GPD-T05	This study
pME5563	p425-GPD-T06	This study

serially diluted 10-fold, and spotted onto SC agar supplemented with glucose or galactose to induce αSyn expression. Plates were incubated for 3 days at 30 °C.

4.10. Growth analysis in liquid culture

For growth test in liquid media cells were grown overnight in 100 μL minimal media containing 2 % raffinose in a clear 96-well plate. The plate was incubated in a Tecan Infinite M200 plate reader at 30 °C with continuous shaking until all samples had grown into stationary phase. The next morning 1 μL from each well was transferred into a new well with 90 μL SC media containing 2 % raffinose and grown for 90 min at 30 °C with continuous shaking. To induce αSyn expression 10 μL 20 % galactose was added to each well and cell growth was observed for 72 h at 30 °C and with continuous shaking. The absorbance at 600 nm was measured every 30 min.

4.11. Fluorescence microscopy

Yeast cells were grown overnight in selective SC medium containing 2 % raffinose and diluted to $OD_{600} = 0.1$ the next morning in SC medium containing 2 % galactose to induce αSyn expression. After 6 h the cells were transferred into 8-well Ibidi Dishes (Ibidi, Gräfeling, Germany) and imaged using a Zeiss Observer Z1 microscopy (Carl Zeiss, Oberkochen, Germany) equipped with a CSU-X1 A1 confocal scanner unit (YOKOGAWA, Musashino, Japan) and a QuantEM:512SC digital camera (Teledyne Photometrics, Tucson, AZ). For the quantification of cells with αSyn aggregates, 100 cells were counted per sample and 3 independent experiments were performed per sample.

4.12. Flow cytometry

Cells were grown overnight in SC medium with 2 % raffinose and inoculated at OD of 0.3 in SC media containing 2 % galactose on the following day for 6h. Cells were washed and re-suspended in 50 mM trisodium citrate buffer (pH 7.0). The integrity of the yeast cell membrane was analyzed using propidium iodide (PI) (Thermo Fischer, Waltham, MA) staining. Yeast cells were incubated with 12.5 μg/mL PI for 30 min at 30 °C in the dark. Flow cytometry was performed using a BD FACSANTO II (Becton Dickinson, Franklin Lakes, NJ), counting 10000 events for each experiment. The data were analyzed using BD FACSDIVA software (Becton Dickinson, Franklin Lakes, NJ).

4.13. Human cells

Human neuroglioma cells (H4) were maintained at 37 °C and 5 % CO_2 in Opti-MEM I Reduced Serum Medium (Life Technologies-Ginco, Carlsbad, CA), which was supplemented with 10 % fetal bovine serum GOLD (FBS) (PAA, Cölbe, Germany) and 1 % Penicillin-Streptomycin. 24 h before transfection the cells were plated in 12-well plates (Costar, Corning, New York), and transfection was performed using FuGENE® transfection reagent (Promega, Madison, WI) according to the manufacturer's instructions. The plasmids coding for SynT and synphilin-1 were used in a ratio of 1:1 as previously described [39]. Cells were treated with synthesized peptides 6 h after transfection at a concentration of 10 μM for 42 h before being fixed for immunocytochemistry.

4.14. Immunocytochemistry

Immunocytochemistry protocol was adapted from Ref. [58] using 4 % paraformaldehyde in Dulbecco's Phosphate Buffered Saline (DBPS) to fixate the cells. Afterward, cells were washed 3 times in DBPS, blocked, and simultaneously permeabilized for 30 min at room temperature using 1,5 % normal goat serum (S1000, Vector) and 0.1 % Triton X-100 in DPBS. Cells were washed and incubated overnight at 4 °C with the primary anti-αSyn antibody (Syn1, 1:1000, BD Transduction Laboratory, USA). After washing the cells with 1xPBS, the cells were incubated with a secondary antibody (Alexa Fluor 488 donkey anti-mouse IgG; Life Technologies-Invitrogen, USA) for 1 h at RT. Finally, cells were stained with DAPI (Carl Roth, Germany) for 5 min. Subsequently, coverslips were mounted onto microscope slides, treated with Fluoromount-G (Life Technologies-Invitrogen, USA), and allowed to dry. The slides were then stored at RT until further imaging and analysis.

4.15. Statistical analysis

Data were analyzed using GraphPad Prism 6 software (San Diego, California, USA) and were presented as mean ± SEM of at least three independent experiments. Statistical significance of differences was calculated using either Student's t-test or one-way ANOVA. Differences were considered significant when the *p*-value was smaller than 0.05.

CRediT authorship contribution statement

Tariq T. Ali: Writing – original draft, Visualization, Methodology, Investigation, Formal analysis, Conceptualization. **Madiha Merghani:** Investigation. **Mohammed Al-Azzani:** Investigation. **Luisa Maria Gatzemeier:** Investigation. **Michael Hoppert:** Resources, Investigation. **Dora Kaloyanova:** Resources, Investigation. **Tiago F. Outeiro:** Writing – review & editing, Resources. **Piotr Neumann:** Writing – review & editing, Software, Resources. **Blagovesta Popova:** Writing – review & editing, Writing – original draft, Supervision, Project administration, Methodology, Investigation, Conceptualization. **Gerhard H. Braus:** Writing – review & editing, Writing – original draft, Supervision, Resources, Funding acquisition.

Funding

This work is supported by Deutsche Forschungsgemeinschaft (DFG: BR 1502/18-2) to Gerhard H. Braus.

Declaration of competing interest

The authors declare that they have no known competing financial interests or personal relationships that could have appeared to influence the work reported in this paper.

Acknowledgements

We thank Fabian Rabe von Pappenheim for his assistance with circular dichroism measurements, and Ariane Trapp for excellent technical support. We thank Renée Groetjes for DLS measurements on the Prometheus Panta that were done at the Protein Research Centre of Utrecht University.

Appendix A. Supplementary data

Supplementary data to this article can be found online at https://doi.org/10.1016/j.ejmech.2025.117452.

Abbreviations

αSyn, α-synuclein; CD, circular dichroism; EDTA, ethylenediaminetetraacetic acid; SDS-PAGE, sodium dodecyl sulfate-polyacrylamide gel electrophoresis; ThT, Thioflavin-T dye; DLS, dynamic light scattering; PD, Parkinson's disease; LBs, Lewy bodies; NAC, non-amyloid β component; ISc, interface score; CFP, cyan fluorescent protein; TEM, transmission electron microscopy; SC, synthetic complete dropout; PI, propidium iodide.

Data availability

Data will be made available on request.

References

[1] P. Alam, L. Bousset, R. Melki, D.E. Otzen, A-synuclein oligomers and fibrils: a spectrum of species, a spectrum of toxicities, J. Neurochem. (2019) 522–534, https://doi.org/10.1111/jnc.14808.

[2] R. Balestrino, A.H.V. Schapira, Parkinson disease, Eur. J. Neurol. 27 (2020) 27–42, https://doi.org/10.1111/ene.14108.

[3] H.R. Morris, M.G. Spillantini, C.M. Sue, C.H. Williams-Gray, The pathogenesis of Parkinson's disease, Lancet 403 (2024) 293–304, https://doi.org/10.1016/S0140-6736(23)01478-2.

[4] M.G. Spillantini, M.L. Schmidt, V.M.Y. Lee, J.Q. Trojanowski, R. Jakes, M. Goedert, α-synuclein in Lewy bodies, Nature 388 (1997) 839–840, https://doi.org/10.1038/42166.

[5] R. Krüger, W. Kuhn, T. Müller, D. Woitalla, M. Graeber, S. Kösel, H. Przuntek, J. T. Epplen, L. Schöls, O. Riess, Ala30Pro mutation in the gene encoding α-synuclein in Parkinson's disease, Nat. Genet. 18 (1998) 106–108, https://doi.org/10.1038/ng0298-106.

[6] M.H. Polymeropoulos, C. Lavedan, E. Leroy, S.E. Ide, A. Dehejia, A. Dutra, B. Pike, H. Root, J. Rubenstein, R. Boyer, E.S. Stenroos, S. Chandrasekharappa, A. Athanassiadou, T. Papapetropoulos, W.G. Johnson, A.M. Lazzarini, R. C. Duvoisin, G. Di Iorio, L.I. Golbe, R.L. Nussbaum, Mutation in the α-synuclein gene identified in families with Parkinson's disease, Science 276 (1997) 2045–2047.

[7] H. Yoshino, M. Hirano, A.J. Stoessl, Y. Imamichi, A. Ikeda, Y. Li, M. Funayama, I. Yamada, Y. Nakamura, V. Sossi, M.J. Farrer, K. Nishioka, N. Hattori, Homozygous alpha-synuclein p.A53V in familial Parkinson's disease, Neurobiol. Aging 57 (2017), https://doi.org/10.1016/J.NEUROBIOLAGING.2017.05.022, 248.e7-248.e12.

[8] J.J. Zarranz, J. Alegre, J.C. Gómez-Esteban, E. Lezcano, R. Ros, I. Ampuero, L. Vidal, J. Hoenicka, O. Rodriguez, B. Atarés, V. Llorens, E. Gomez Tortosa, T. Del Ser, D.G. Muñoz, J.G. De Yebenes, The new mutation, E46K, of α-synuclein causes Parkinson and Lewy body dementia, Ann. Neurol. 55 (2004) 164–173, https://doi.org/10.1002/ANA.10795.

[9] S. Lesage, M. Anheim, F. Letournel, L. Bousset, A. Honoré, N. Rozas, L. Pieri, K. Madiona, A. Dürr, R. Melki, C. Verny, A. Brice, G51D α-synuclein mutation causes a novel Parkinsonian–pyramidal syndrome, Ann. Neurol. 73 (2013) 459–471, https://doi.org/10.1002/ANA.23894.

[10] S. Appel-Cresswell, C. Vilarino-Guell, M. Encarnacion, H. Sherman, I. Yu, B. Shah, D. Weir, C. Thompson, C. Szu-Tu, J. Trinh, J.O. Aasly, A. Rajput, A.H. Rajput, A. Jon Stoessl, M.J. Farrer, Alpha-synuclein p.H50Q, a novel pathogenic mutation for Parkinson's disease, Mov. Disord. 28 (2013) 811–813, https://doi.org/10.1002/MDS.25421.

[11] M.C. Chartier-Harlin, J. Kachergus, C. Roumier, V. Mouroux, X. Douay, S. Lincoln, C. Levecque, L. Larvor, J. Andrieux, M. Hulihan, N. Waucquier, L. Defebvre, P. Amouyel, M. Farrer, A. Destée, α-synuclein locus duplication as a cause of familial Parkinson's disease, Lancet 364 (2004) 1167–1169, https://doi.org/10.1016/S0140-6736(04)17103-1.

[12] A.B. Singleton, M. Farrer, J. Johnson, A. Singleton, S. Hague, J. Kachergus, M. Hulihan, T. Peuralinna, A. Dutra, R. Nussbaum, S. Lincoln, A. Crawley, M. Hanson, D. Maraganore, C. Adler, M.R. Cookson, M. Muenter, M. Baptista, D. Miller, J. Blancato, J. Hardy, K. Gwinn-Hardy, α-Synuclein locus triplication causes Parkinson's disease, Science 302 (2003) 841, https://doi.org/10.1126/science.1090278.

[13] S. Mehra, S. Sahay, S.K. Maji, α-Synuclein misfolding and aggregation: implications in Parkinson's disease pathogenesis, Biochim. Biophys. Acta, Proteins Proteomics 1867 (2019) 890–908, https://doi.org/10.1016/j.bbapap.2019.03.001.

[14] B. Winner, R. Jappelli, S.K. Maji, P.A. Desplats, L. Boyer, S. Aigner, C. Hetzer, T. Loher, M. Vilar, S. Campioni, C. Tzitzilonis, A. Soragni, S. Jessberger, H. Mira, A. Consiglio, E. Pham, E. Masliah, F.H. Gage, R. Riek, In vivo demonstration that α-synuclein oligomers are toxic, Proc. Natl. Acad. Sci. U. S. A 108 (2011) 4194–4199, https://doi.org/10.1073/PNAS.1100976108.

[15] D. Emin, Y.P. Zhang, E. Lobanova, A. Miller, X. Li, Z. Xia, H. Dakin, D.I. Sideris, J.Y. L. Lam, R.T. Ranasinghe, A. Kouli, Y. Zhao, S. De, T.P.J. Knowles, M. Vendruscolo, F.S. Ruggeri, F.I. Aigbirhio, C.H. Williams-Gray, D. Klenerman, Small soluble α-synuclein aggregates are the toxic species in Parkinson's disease, Nat. Commun. 13 (2022) 1–15, https://doi.org/10.1038/s41467-022-33252-6.

[16] N. Bengoa-Vergniory, R.F. Roberts, R. Wade-Martins, J. Alegre-Abarrategui, Alpha-synuclein oligomers: a new hope, Acta Neuropathol. 134 (2017) 819–838, https://doi.org/10.1007/s00401-017-1755-1.

[17] A. Jan, N.P. Gonçalves, C.B. Vaegter, P.H. Jensen, N. Ferreira, The prion-like spreading of alpha-synuclein in Parkinson's disease: update on models and hypotheses, Int. J. Mol. Sci. 22 (2021) 8338, https://doi.org/10.3390/ijms22158338.

[18] P. Arosio, T.P.J. Knowles, S. Linse, On the lag phase in amyloid fibril formation, Phys. Chem. Chem. Phys. 17 (2015) 7606–7618, https://doi.org/10.1039/C4CP05563B.

[19] S. Mehra, L. Gadhe, R. Bera, A.S. Sawner, S.K. Maji, Structural and functional insights into α-synuclein fibril polymorphism, Biomolecules 11 (2021), https://doi.org/10.3390/biom11101419.

[20] B. Li, P. Ge, K.A. Murray, P. Sheth, M. Zhang, G. Nair, M.R. Sawaya, W.S. Shin, D. R. Boyer, S. Ye, D.S. Eisenberg, Z.H. Zhou, L. Jiang, Cryo-EM of full-length α-synuclein reveals fibril polymorphs with a common structural kernel, Nat. Commun. 9 (2018) 3609, https://doi.org/10.1038/s41467-018-05971-2.

[21] T. Srivastava, D. Tyagi, S. Fatima, M. Thirumalesh, V. Sathyan, R. Raj, Aniket Sharma, M. Chaturvedi, M. Sinha, S.K. Shishodia, Dinesh Kumar, S. K. Sharma, J. Shankar, A. Satish, S. Priya, A natural small molecule-mediated inhibition of alpha-synuclein aggregation leads to neuroprotection in Caenorhabditis elegans, J. Neurochem. 168 (2024) 1–15, https://doi.org/10.1111/JNC.15907.

[22] J. Pujols, S. Peña-Díaz, D.F. Lázaro, F. Peccati, F. Pinheiro, D. González, A. Carija, S. Navarro, M. Conde-Giménez, J. García, S. Guardiola, E. Giralt, X. Salvatella, J. Sancho, M. Sodupe, T.F. Outeiro, E. Dalfó, S. Ventura, Small molecule inhibits α-synuclein aggregation, disrupts amyloid fibrils, and prevents degeneration of dopaminergic neurons, Proc. Natl. Acad. Sci. U. S. A 115 (2018) 10481–10486, https://doi.org/10.1073/pnas.1804198115.

[23] B.D. Khairnar, A. Jha, J.M. Rajwade, Rationally designed cyclic peptides and nanomaterials as 'next-generation' anti-amyloid therapeutics, J. Mater. Sci. 58 (2023) 9834–9860, https://doi.org/10.1007/s10853-023-08654-6.

[24] S. Sangwan, S. Sahay, K.A. Murray, S. Morgan, E.L. Guenther, L. Jiang, C. K. Williams, H.V. Vinters, M. Goedert, D.S. Eisenberg, Inhibition of synucleinopathic seeding by rationally designed inhibitors, Elife 9 (2020), https://doi.org/10.7554/ELIFE.46775.

[25] J.H. Torpey, R.M. Meade, R. Mistry, J.M. Mason, J. Madine, Insights into peptide inhibition of alpha-synuclein aggregation, Front. Neurosci. 14 (2020) 1082, https://doi.org/10.3389/fnins.2020.561462.

[26] C. Wang, S. Shao, N. Li, Z. Zhang, H. Zhang, B. Liu, Advances in alzheimer's disease-associated Aβ therapy based on peptide, Int. J. Mol. Sci. 24 (2023), https://doi.org/10.3390/IJMS241713110.

[27] B. Popova, D. Wang, A. Rajavel, K. Dhamotharan, D.F. Lázaro, J. Gerke, J.F. Uhrig, M. Hoppert, T.F. Outeiro, G.H. Braus, Identification of two novel peptides that inhibit α-synuclein toxicity and aggregation, Front. Mol. Neurosci. 14 (2021) 54, https://doi.org/10.3389/FNMOL.2021.659926.

[28] Y. Li, C. Zhao, F. Luo, Z. Liu, X. Gui, Z. Luo, X. Zhang, D. Li, C. Liu, X. Li, Amyloid fibril structure of α-synuclein determined by cryo-electron microscopy, Cell Res. 28 (2018) 897–903, https://doi.org/10.1038/s41422-018-0075-x.

[29] K.T. Simons, R. Bonneau, I. Ruczinski, D. Baker, Ab initio protein structure prediction of CASP III targets using ROSETTA, Proteins Struct. Funct. Genet. 37 (1999) 171–176, https://doi.org/10.1002/(SICI)1097-0134(1999)37:3+<171::AID-PROT21>3.0.CO;2-Z.

[30] D.E. Kim, D. Chivian, D. Baker, Protein structure prediction and analysis using the Robetta server, Nucleic Acids Res. 32 (2004), https://doi.org/10.1093/nar/gkh468.

[31] C. Louis-Jeune, M.A. Andrade-Navarro, C. Perez-Iratxeta, Prediction of protein secondary structure from circular dichroism using theoretically derived spectra, Proteins Struct, Funct. Bioinforma. 80 (2012) 374–381, https://doi.org/10.1002/PROT.23188.

[32] S. Willingham, T.F. Outeiro, M.J. DeVit, S.L. Lindquist, P.J. Muchowski, Yeast genes that enhance the toxicity of a mutant huntingtin fragment or alpha-synuclein, Science 302 (2003) 1769–1772.

[33] T.F. Outeiro, S. Lindquist, Yeast cells provide insight into alpha-synuclein biology and pathobiology, Science 302 (2003) 1772–1775, https://doi.org/10.1126/science.1090439.

[34] D. Petroi, B. Popova, N. Taheri-Talesh, S. Irniger, H. Shahpasandzadeh, M. Zweckstetter, T.F. Outeiro, G.H. Braus, Aggregate clearance of alpha-synuclein in Saccharomyces cerevisiae depends more on autophagosome and vacuole function than on the proteasome, J. Biol. Chem. 287 (2012) 27567–27579, https://doi.org/10.1074/jbc.M112.361865. M112.361865[pii].

[35] A.A. Cooper, A.D. Gitler, A. Cashikar, C.M. Haynes, K.J. Hill, B. Bhullar, K. Liu, K. Xu, K.E. Strathearn, F. Liu, S. Cao, K.A. Caldwell, G.A. Caldwell, G. Marsischky, R.D. Kolodner, J. LaBaer, J.C. Rochet, N.M. Bonini, S. Lindquist, α-synuclein blocks ER-Golgi traffic and Rab1 rescues neuron loss in Parkinson's models, Science 313 (2006) 324–328, https://doi.org/10.1126/science.1129462.

[36] F. Madeira, Y. Park, J. Lee, et al., The EMBL-EBI search and sequence analysis tools APIs in 2019, Nucleic Acids Res. 47 (2019) W636–W641, https://doi.org/10.1093/NAR/GKZ268.

[37] M.L. Duennwald, S. Jagadish, P.J. Muchowski, S. Lindquist, Flanking sequences profoundly alter polyglutamine toxicity in yeast, Proc. Natl. Acad. Sci. USA 103 (2006) 11045–11050, https://doi.org/10.1073/pnas.0604547103.

[38] C. Masaracchia, A. König, A.A. Valiente-Gabioud, P. Peralta, F. Favretto, T. Strohäker, D.F. Lázaro, M. Zweckstetter, C.O. Fernandez, T.F. Outeiro, Molecular characterization of an aggregation-prone variant of alpha-synuclein used to model

synucleinopathies, Biochim. Biophys. Acta, Proteins Proteomics 1868 (2020) 140298, https://doi.org/10.1016/J.BBAPAP.2019.140298.
[39] D.F. Lázaro, E.F. Rodrigues, R. Langohr, H. Shahpasandzadeh, T. Ribeiro, P. Guerreiro, E. Gerhardt, K. Kröhnert, J. Klucken, M.D. Pereira, B. Popova, N. Kruse, B. Mollenhauer, S.O. Rizzoli, G.H. Braus, K.M. Danzer, T.F. Outeiro, Systematic comparison of the effects of alpha-synuclein mutations on its oligomerization and aggregation, PLoS Genet. 10 (2014) e1004741, https://doi.org/10.1371/journal.pgen.1004741.
[40] D.P. Karpinar, M.B.G. Balija, S. Kügler, F. Opazo, N. Rezaei-Ghaleh, N. Wender, H. Y. Kim, G. Taschenberger, B.H. Falkenburger, H. Heise, A. Kumar, D. Riedel, L. Fichtner, A. Voigt, G.H. Braus, K. Giller, S. Becker, A. Herzig, M. Baldus, H. Jäckle, S. Eimer, J.B. Schulz, C. Griesinger, M. Zweckstetter, Pre-fibrillar α-synuclein variants with impaired B-structure increase neurotoxicity in Parkinson's disease models, EMBO J. 28 (2009) 3256–3268, https://doi.org/10.1038/emboj.2009.257.
[41] K.N.L. Huggins, M. Bisaglia, L. Bubacco, M. Tatarek-Nossol, A. Kapurniotu, N. H. Andersen, Designed hairpin peptides interfere with amyloidogenesis pathways: fibril formation and cytotoxicity inhibition, interception of the preamyloid state, Biochemistry 50 (2011) 8202–8212, https://doi.org/10.1021/bi200760h.
[42] L. Wang, N. Wang, W. Zhang, X. Cheng, Z. Yan, G. Shao, X. Wang, R. Wang, C. Fu, Therapeutic peptides: current applications and future directions, Signal Transduct. Targeted Ther. 7 (2022) 1–27, https://doi.org/10.1038/s41392-022-00904-4.
[43] K. Fosgerau, T. Hoffmann, Peptide therapeutics: current status and future directions, Drug Discov. Today 20 (2015) 122–128, https://doi.org/10.1016/j.drudis.2014.10.003.
[44] M.H. Baig, K. Ahmad, M. Saeed, A.M. Alharbi, G.E. Barreto, G.M. Ashraf, I. Choi, Peptide based therapeutics and their use for the treatment of neurodegenerative and other diseases, Biomed. Pharmacother. 103 (2018) 574–581, https://doi.org/10.1016/j.biopha.2018.04.025.
[45] B. Jiang, F. Han, M.H. Lü, Z.P. Wang, W. Liu, Y.X. Zhang, J. Xu, R.J. Li, Bis-chalcone polyphenols with potential preventive and therapeutic effects on PD: design, synthesis and in vitro disaggregation activity against α-synuclein oligomers and fibrils, Eur. J. Med. Chem. 239 (2022), https://doi.org/10.1016/j.ejmech.2022.114529.
[46] S.C. Owen, A.K. Doak, A.N. Ganesh, L. Nedyalkova, C.K. McLaughlin, B. K. Shoichet, M.S. Shoichet, Colloidal drug formulations can explain "bell-shaped" concentration-response curves, ACS Chem. Biol. 9 (2014) 777–784, https://doi.org/10.1021/cb4007584.
[47] T.A. Thibaudeau, R.T. Anderson, D.M. Smith, A common mechanism of proteasome impairment by neurodegenerative disease-associated oligomers, Nat. Commun. 9 (2018) 1097, https://doi.org/10.1038/s41467-018-03509-0.
[48] E. Rockenstein, S. Nuber, C.R. Overk, K. Ubhi, M. Mante, C. Patrick, A. Adame, M. Trejo-Morales, J. Gerez, P. Picotti, P.H. Jensen, S. Campioni, R. Riek, J. Winkler, F.H. Gage, B. Winner, E. Masliah, Accumulation of oligomer-prone α-synuclein exacerbates synaptic and neuronal degeneration in vivo, Brain 137 (2014) 1496–1513, https://doi.org/10.1093/brain/awu057.
[49] M. Goedert, B. Falcon, F. Clavaguera, M. Tolnay, Prion-like mechanisms in the pathogenesis of tauopathies and synucleinopathies, Curr. Neurol. Neurosci. Rep. 14 (2014) 495, https://doi.org/10.1007/s11910-014-0495-z.
[50] K.A. Porter, B. Xia, D. Beglov, T. Bohnuud, N. Alam, O. Schueler-Furman, D. Kozakov, ClusPro PeptiDock: efficient global docking of peptide recognition motifs using FFT, Bioinformatics 33 (2017) 3299–3301, https://doi.org/10.1093/bioinformatics/btx216.
[51] J.J. Gray, S. Moughon, C. Wang, O. Schueler-Furman, B. Kuhlman, C.A. Rohl, D. Baker, Protein-protein docking with simultaneous optimization of rigid-body displacement and side-chain conformations, J. Mol. Biol. 331 (2003) 281–299, https://doi.org/10.1016/S0022-2836(03)00670-3.
[52] S. Chaudhury, M. Berrondo, B.D. Weitzner, P. Muthu, H. Bergman, J.J. Gray, Benchmarking and analysis of protein docking performance in Rosetta v3.2, PLoS One 6 (2011) e22477, https://doi.org/10.1371/JOURNAL.PONE.0022477.
[53] G.S. Vanier, Microwave-assisted solid-phase peptide synthesis based on the Fmoc protecting group strategy (CEM), Methods Mol. Biol. 1047 (2013) 235–249, https://doi.org/10.1007/978-1-62703-544-6_17.
[54] L. Giehm, D.E. Otzen, Strategies to increase the reproducibility of protein fibrillization in plate reader assays, Anal. Biochem. 400 (2010) 270–281, https://doi.org/10.1016/J.AB.2010.02.001.
[55] M. Hoppert, A. Holzenburg, Electron Microscopy in Microbiology (Bios, Scientific Publ, Oxford, UK, 1998.
[56] D. Gietz, A. St Jean, R.A. Woods, R.H. Schiestl, Improved method for high efficiency transformation of intact yeast cells, Nucleic Acids Res. 20 (1992) 1425.
[57] D. Mumberg, R. Muller, M. Funk, R. Müller, M. Funk, Regulatable promoters of Saccharomyces cerevisiae: comparison of transcriptional activity and their use for heterologous expression, Nucleic Acids Res. 22 (1994) 5767–5768.
[58] E.C. Schulte, D.C. Ellwanger, S. Dihanich, C. Manzoni, K. Stangl, B. Schormair, E. Graf, S. Eck, B. Mollenhauer, D. Haubenberger, W. Pirker, A. Zimprich, T. Brücke, P. Lichtner, A. Peters, C. Gieger, C. Trenkwalder, H.W. Mewes, T. Meitinger, P.A. Lewis, H.H. Klünemann, J. Winkelmann, Rare variants in LRRK1 and Parkinson's disease, Neurogenetics 15 (2014) 49–57, https://doi.org/10.1007/S10048-013-0383-8.